Applied Catalysis B: Environmental 324 (2023) 122201

Contents lists available at ScienceDirect

Applied Catalysis B: Environmental

journal homepage: www.elsevier.com/locate/apcatb

Highly selective nitrate reduction to ammonia on CoO/Cu foam via constructing interfacial electric field to tune adsorption of reactants

Wenyang Fu [a,b,c], Yingying Du [a,b,c], Jiana Jing [a,b,c], Chunhong Fu [a,b,c], Minghua Zhou [a,b,c,*]

[a] Key Laboratory of Pollution Process and Environmental Criteria, Ministry of Education, College of Environmental Science and Engineering, Nankai University, Tianjin 300350, China
[b] Tianjin Key Laboratory of Environmental Technology for Complex Trans-Media Pollution, Nankai University, Tianjin 300350, China
[c] Tianjin Advanced Water Treatment Technology International Joint Research Center, College of Environmental Science and Engineering, Nankai University, Tianjin 300350, China

ARTICLE INFO

Keywords:
ERNA
CoO/Cu foam electrode
Interfacial electric field
NO3− adsorption
NO adsorption

ABSTRACT

Electrochemical reduction of nitrate to ammonia (ERNA) is a new process to recycle nitrogen resource from nitrate polluted wastewater. Nevertheless, how to optimize active sites on electrode to improve activity is a key challenge. Here, we proposed that building interfacial electric field could enhance ERNA. XPS analysis, DFT calculations and in-situ electrochemical measurements confirmed that high Fermi level of Cu (1.09 eV) and low valence band maximum of CoO (−0.23 eV) formed interfacial electric field in CoO/Cu electrode to transfer electron from Cu to CoO, resulting in positively charged Cu (+0.01 eV) increase nitrate adsorption, whereas negatively charged CoO (−0.007 eV) decrease NO adsorption, improving removal and selectivity greatly for boosting ERNA. Eventually, CoO/Cu foam (Co/Cu ratio of 3.05) achieved the highest ammonia yield of 4.3 mg cm^{-2} h^{-1} with faradic efficiency of 96.7 %, surpassing Cu foam (1.2 mg cm^{-2} h^{-1}) and CoO/Ni foam (1.3 mg cm^{-2} h^{-1}) electrodes.

1. Introduction

Electrochemical reduction of nitrate to ammonia (ERNA) has become an important issue for removal of nitrate (NO_3^-) contaminant and ammonia synthesis [1,2]. ERNA has become a kind of new green and low-carbon technology for ammonia synthesis via reducing NO_3^- contaminant without discharge of CO_2, altering haber-bosch process with high energy consumption and CO_2 emission to provide sustainable ammonia to factory from wastewater [3]. Owning to the activity of human being, NO_3^- is extensively distributed in the environment [4]. Particularly, some industrial wastewaters have high concentration of NO_3^- ($C_{NO_3^-}$), such as chemical industrial wastewater with $C_{NO_3^-}$ of 241–2527 mg L^{-1} and actual industrial wastewater with $C_{NO_3^-}$ of 2579 mg L^{-1} (0.041 M) [5,6]. Thereby, it is significant to treat industrial wastewater for recycling nitrogen resource via ERNA to synthesis NH_3, simultaneously solving problem of environmental pollution.

Nevertheless, ERNA process is still inhibited by developing high-activity and low-cost non-noble electrodes. The previous work demonstrated Cu was the most efficient non-noble material [7–10], whereas Cu produced plenty of NO_2^- in ERNA [11,12]. Building dual active sites can improve activity of Cu electrode. For example, Cu/Mn_3O_4 electrode achieved ammonia selectivity of 87.6 % with faradic efficiency of 92.4 % due to its synergy of nano-interface and oxygen vacancies [13]. But little attention has been paid to the effect of interfacial electric field on dual active site in ERNA. It was demonstrated that built-in electric field between TiO_2 and CuCl could accumulate nitrate and decline energy barrier of reduction of *NO intermediate to boost ERNA [14]. However, it was barely noted that built-in electric field could help electrons to transfer from TiO_2 to CuCl, resulting in positively charged TiO_2 and negatively charged CuCl to affect the activity of ERNA [14]. The charge of active sites was important for ERNA because the positively charged active sites were beneficial for enhancing the adsorption of nitrate with negative charge. For instance, constructing the oxygen defect could make active sites become a little positive, facilitating the adsorption of nitrate to increase activity [15]. In addition, previous work reported that electrode interacted weakly with NO intermediate, improving selectivity of reducing NO_3^- to NH_3 [16]. Moreover, the negatively charged active site was good at reducing the adsorption of key intermediates. For

* Corresponding author at: Key Laboratory of Pollution Process and Environmental Criteria, Ministry of Education, College of Environmental Science and Engineering, Nankai University, Tianjin 300350, China.
E-mail address: zhoumh@nankai.edu.cn (M. Zhou).

https://doi.org/10.1016/j.apcatb.2022.122201
Received 29 August 2022; Received in revised form 29 October 2022; Accepted 19 November 2022
Available online 21 November 2022

example, negatively charged Ni_3S_2 in Cu nanodots-decorated Ni_3S_2 nanotubes could decrease adsorption of H_{ads} to improve ability of hydrogen evolution [17]. Therefore, regulating the charge of active sites maybe increase the adsorption of nitrate and decrease adsorption of key intermediates to enhance the reactivity of ERNA.

The charge of active sites can be adjusted via the interfacial electric field formed at the interface due to difference of energy level when two phase contacted [18]. Controlling energy difference of the interfacial electric field can manage the electrons transfer from one active site to another and tune the electron distribution of the active site. It had been proved that the interface formed by metal and metal oxides could produce strong metal-support interaction (SMSI), which can form the interfacial electric field [19–21]. Similarly, supporting of metal oxides on metals could also produce the interfacial electric field [22]. Moreover, some previous studies had demonstrated that the CoO based electrode had a good ability of converting NO_3^- into NH_3, but individual CoO had relatively low activity in ERNA [23–25]. Thus, CoO could be used as metal oxides, combining with Cu to build interfacial electric field to improve activity. Meanwhile, considering that the complex fiber structure of the copper foam can be used to provide more active areas [26], Cu foam should be a good supporter to loading CoO on Cu foam, and it is necessary to investigate the effect of interfacial electric field on the ERNA performance.

This study focused on the effect of interfacial electric field on charge distribution of active sites for enhancement of ERNA, and provide a sound strategy to optimize dual active sites electrodes. Cobalt oxide (II)/copper foam (CoO/Cu foam) electrode was prepared by electrodeposition and high temperature calcination under argon atmosphere. XPS analysis and density functional theory (DFT) calculations were used to prove the existence of the interfacial electric field to adjust charge distribution of active site. And then, XPS, DFT calculations, in-situ fourier transform infrared spectroscopy (in-situ FTIR) and differential electrochemical mass spectrometry (DEMS) clarified the influence of the charge distribution of Cu foam and CoO in CoO/Cu foam electrode on the enhancement of ERNA. Eventually, this work demonstrated that regulating the interfacial electric field was a reliable method for boosting ERNA activity via changing charge distribution of active sites.

2. Materials and methods

2.1. Materials

Cu foam was supplied from Kunshan Xingzhenghong Electronic Materials Co., Ltd (China). Ni foam was bought from Suzhou Sinero Technology Co., Ltd (China). $Co(NO_3)_2{\cdot}6H_2O$, $Na_2Fe(CN)_5NO{\cdot}2H_2O$ (sodium nitroferricyanide(III) dihydrate), C_6H_4OH (phenol), C_2H_6O (ethanol), formic acid, C_3H_6O (acetone), NaClO, isopropanol and $C_6H_5Na_3O_7$ (trisodium citrate dihydrate) were obtained from Aladdin Co., Ltd (China), Na_2SO_4, NaOH, $NaNO_3$, NaOH, HNO_3, NH_4Cl, and $NaNO_2$ were purchased from Tianjin Chemart Chemical science and technology Co., Ltd (China). Commercially available dimensionally stable anode (DSA) electrodes were purchased from Baoji Changli Co. Ltd (China).

2.2. Preparation of CoO/Cu foam and CoO/Ni foam

Cu foam (round, 6 cm^2) was ultrasonically washed three times in acetone. And then, it was ultrasonically washed in 0.1 mol L^{-1} H_2SO_4 for 3 min. Next, Cu foam was washed with distilled water until the washing water became neutral, and dried in a vacuum drying oven at 60 °C. The dried Cu foam was then placed in a plating bath for electrodeposition. A three-electrode cell was used for electrodeposition, the working electrode was Cu foam, the reference electrode was Ag/AgCl electrode, and the counter electrode was carbon rod. The electrodeposition solution was 7.2 g L^{-1} of cobalt nitrate solution. The electrodeposition method was chronopotentiometry, and the current was 40 mA with electrodepositing time of 120 min, obtaining a $Co(OH)_2$/Cu foam electrode, which was then simply rinsed with distilled water, and then dried naturally. The dried electrodes were placed in a tube furnace for calcination at temperature of 600 °C with the heating rate of 5 °C min^{-1} in argon atmosphere with the gas flow of 50 mL min^{-1}. After 3 h of calcination, CoO/Cu foam electrode was obtained.

The fabrication of CoO/Ni foam electrode was similar to CoO/Cu foam except Ni foam (nickel foam) as the support. Ni foam was also rinsed with acetone, H_2SO_4 solution and distilled water in turn. Ni foam was used as the working electrode in electrodepositing to form Co $(OH)_2$/Ni foam electrode, and then $Co(OH)_2$/Ni foam was calcined at 800 °C in argon atmosphere to get CoO/Ni foam electrode.

2.3. Electrochemical measurements

The electrode activity for ERNA was measured via a three-electrodes configuration with CHI 760E electrochemical potentiostat. The working electrode was CoO/Cu foam, CoO/Ni foam or Cu foam (6 cm^2), the counter electrode was a DSA, and the reference electrode was Ag/AgCl electrode, respectively. The potential was set at − 1.2 V vs. Ag/AgCl, and the electrolyte was an argon-saturated 0.4 mol L^{-1} Na_2SO_4 solution including 0.04 mol L^{-1} (2480 mg L^{-1}) NO_3^- with the reactor volume of 25 mL. Moreover, the electrolysis time was 35 min. Electrochemical measurements were CV (cyclic voltammetry), LSV (linear sweep voltammetry), and EIS (electrochemical impedance spectroscopy), respectively. The electrochemical test system also adopted a three-electrodes configuration: CoO/Cu foam was used as working electrode, Pt sheet was used as counter electrode, and Ag/AgCl was used as reference electrode. The active area of the working electrode was 1 cm × 1 cm. The reactor is a single electrolytic cell with volume of 250 mL. The electrolyte was 0.4 mol L^{-1} Na_2SO_4 with or without 0.04 mol L^{-1} NO_3^-. All electrolyte was deoxidized by argon gas for half an hour before measurements.

In addition, electrochemical surface area (ECSA). ECSA was calculated by followed equation:

$$C_{dl} = \frac{I}{v} \tag{1}$$

$$\text{ECSA} = \frac{C_{dl}}{C * \times A} \tag{2}$$

where C_{dl} is capacitance of double layer of electrode (F), I is current (A) in CV, v is scan rate (V s^{-1}), C^* is the specific capacitance of ideal smooth oxide (60 μF cm^{-2}).

2.4. Characterizations

The morphology of electrode was studied via scanning electron microscope (SEM) of LEO-1530VP (Carl Zeiss AG, Germany). The phase of electrode was identified via X-ray diffraction (XRD) patterns with an X-ray diffractometer of Cu Kα radiation (Rigaku Ultima IV, Japan). The electron transfer of interface on electrode was investigated via X-ray photoelectron spectroscopy (XPS) on a thermos ESCALAB 250 (Thermo Fisher Scientific, USA) with the Al Kα X-rays irradiation ($h\nu$ = 1486.6 eV). The concentration of NO_2^- and NO_3^- was measured through ionic chromatography of Dionex ICS-900 (Thermo Fisher Scientific, USA) with AS20 analytical column under flow rate of 1 mL min^{-1} KOH (mobile phase). The quantity of nitrogenous gas (N_2, N_2O or volatile NH_3) was determined via initial total nitrogen (TN_0) minus total nitrogen at reaction time t (TN_t) in solution, and TN was measured by total organic carbon analysis (TOC-L, SHIMADZU, Japan). The amounts of Co and Cu ions in solution and Co in electrodes were detected by inductively coupled plasma mass spectrometry (ICP-MS, PerkinElmer ELAN DRC-e, USA), and electrode was dissolved in 2 M HNO_3 solution under 80 °C for 12 h to confirm the number of Co in electrode. Indophenol blue method was carried on to obtain the amounts of NH_3 (detailed steps was

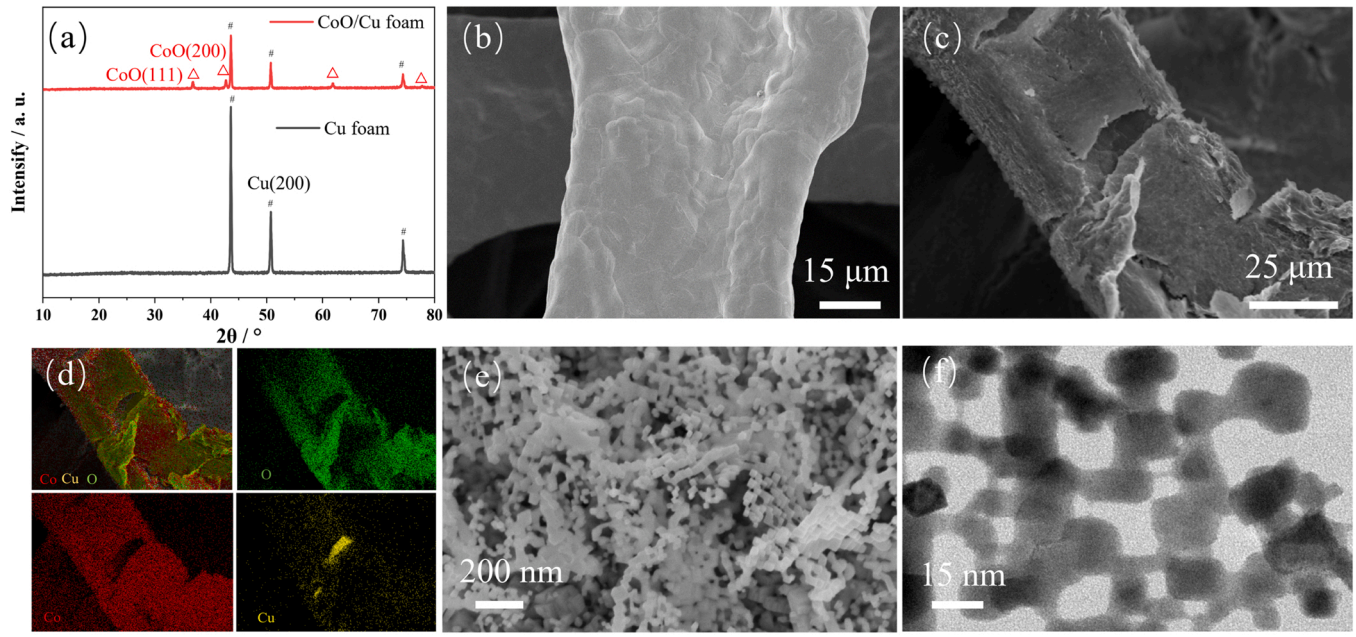

Fig. 1. (a) XRD patterns of CoO/Cu foam and Cu foam electrodes; (b) SEM image of Cu foam electrodes (15 μm); (c) SEM images of CoO/Cu foam electrodes (25 μm); (d) Co, Cu and O elements mapping of CoO/Cu foam electrodes; (e) SEM image of CoO/Cu foam (200 nm); (f) TEM picture of CoO/Cu foam.

shown in supplementary material) [27]. In addition, the selectivity of NH_3 and NO_2^- (S_{NH_3} and $S_{NO_2^-}$) and faraday efficiency (FE) of NH_3 were figured out by [28]:

$$S_{NH_3} = \frac{C_{t(NH_3)}}{C_{0(NO_3^-)} - C_{t(NO_3^-)}} \times 100\ \% \quad (3)$$

$$S_{NO_2^-} = \frac{C_{t(NO_2^-)}}{C_{0(NO_3^-)} - C_{t(NO_3^-)}} \times 100\ \% \quad (4)$$

$$FE = \frac{z \times F \times C_{t(NH_3)} \times V}{Q_t} \times 100\% \quad (5)$$

where $C_{t(NH_3)}$, $C_{t(NO_2^-)}$, $C_{t(NO_3^-)}$ are the mole concentration of NH_3, NO_2^-, and NO_3^- at reaction time t (mol L^{-1}), respectively, $C_{0(NO_3^-)}$ is the NO_3^- at initial time (mol L^{-1}), Z is the number of electron transferred from reducing NO_3^- to NH_3, F is constant of Faraday (96,500 C mol^{-1}). Q_t is quantity at reaction time t (C), V is volume of solution (L). In addition, according to the results of electrochemical differential mass spectrometry (DEMS), it can be known that NO was detected and NH_2OH was not detected. And thus, the selectivity of other products (e. g. NO, N_2 or N_2O) can be calculated by 100 % minus the selectivity of NO_2^- and NH_3 [29,30]:

$$S_{other} = 100\% - S_{NO_2^-} - S_{NH_3} \quad (6)$$

2.5. In-situ electrochemical measurements

In-situ Fourier transformed infrared spectroscopy (in-situ FTIR) was used to study the reaction pathway of ERNA. Infrared spectrometer in in-situ FTIR was performed by Thermo Scientific Nicolet IS50 FTIR (Thermo Fisher Scientific, USA), and this system was external reflection with prism of Si crystal. The electrochemical cell was assembled by a three-electrode configuration with count electrode of Pt wire, reference electrode of Ag/AgCl and working electrode of CoO/Cu foam . The working electrode was pressed via glassy carbon electrode to connect CHI 760E electrochemical potentiostat (Shanghai Chinstrument, China) with electrolysis time of 600 s at − 1.2 *vs*. Ag/AgCl. The electrolyte was 0.4 mol L^{-1} Na_2SO_4 with or without 0.04 mol L^{-1} NO_3^-.

DEMS was used to identified volatile and unstable intermediates in ERNA. Three electrochemical configurations and reaction condition in DEMS were the same as those in in-situ FTIR. Additionally, DEMS were repeated in three continuous cycles within 60 s. To eliminate the accidental error in DEMS measurements, next cycle started when the mass signal declined to baseline after last cycle.

2.6. DFT calculations

Density functional theory (DFT) calculations used Vienna Ab-initio Simulation Package (VASP 5.4.4) software to obtain reaction energy and electronic structure in ERNA. The exchange-correlation potential of electron was described via Perdew-Burke-Ernzerfor (PBE) functional with generalized gradient approximation (GGA) and cut-off energy of 450 eV [31,32]. Notably, the script of VASP-sol used implicit solvation model to simulate solvent effects [33,34]. Considering 200 crystal plane of CoO had high intensity in XRD and the heterojunction model constructed with the same crystal plane is relatively stable, 200 crystal plane of CoO loading on 200 crystal plane of Cu were selected to simulate CoO/Cu electrode with lattice constant of 9 × 8 × 26 (vacuum slab of 15 Å). What's more, the ratio of CoO and Cu in surface of CoO/Cu model was modified by the results of XPS (9 Co atoms and 3 Cu atoms on the surface of convention cell and 9 Co atoms and 33 Cu atoms in convention cell, respectively). For comparison, the model of Cu foam and CoO were 200 crystal planes as well. In particular, to save computing resources, the atoms in the lower two layers of the model were fixed when simulating reactant adsorption structure after the geometry optimization of the material model. 1 × 1 × 1 k points were used for geometry optimization, and 5 × 5 × 3 k points were utilized to obtain energy and electronic structure. All calculations stop when the force below 0.03 eV $Å^{-1}$. The adsorption energy and the Gibbs free-energy were calculated based on previous reported paper [35]. In addition, crystal orbital hamilton populations (COHP) analysis was performed by LOBSTER software [36] and energy of transition state in key step of ERNA was calculated by transition state tools for VASP with the CI-NEB (Climbing Image Nudged-Elastic-Band) method [37].

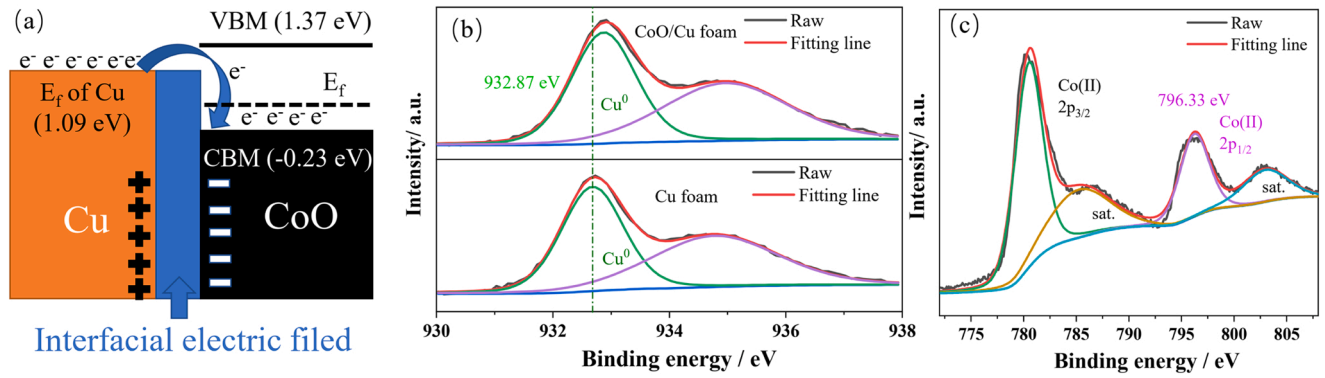

Fig. 2. (a) Schematic illusion of interfacial electric field (Criterion was fermi level (E_f) of CoO); (b) XPS images of Cu 2p orbital of CoO/Cu foam and Cu foam electrodes, respectively; (c) Co 2p orbital of CoO/Cu foam electrode.

3. Results and discussion

3.1. Characterization of CoO/Cu foam electrode

The phase of CoO/Cu foam electrode was confirmed by XRD characterization. Compared with Cu foam, CoO/Cu foam electrode exhibited three peaks at 36.5, 42.4, 61.5 and 77.6° (Fig. 1a), which belonged to the (111), (200), (220) and (222) crystal planes of CoO (PDF#43-1004), respectively. This indicated that CoO/Cu foam electrode was composed of Cu and CoO without other impurities. As shown in Fig. 1b, the structure of Cu foam was uneven Cu fibers with width of about 58 μm. After loading CoO, the surface of Cu foam became significantly rough (Fig. 1c and S1), indicating that CoO loaded on Cu foam. In addition, some cracks were made by uneven surface of Cu foam (Fig. 1b and S1a). Moreover, the corresponding elemental mapping of CoO/Cu foam electrode uncovered that Co, O and Cu elements were relatively uniformly distributed on the surface of CoO/Cu foam electrode (Fig. 1d), indicating that both CoO and Cu exposed on CoO/Cu foam electrode. Furthermore, the small view of SEM image of the CoO/Cu foam revealed that CoO was formed by stacking small particles grown on the surface of Cu foam (Fig. 1e). And TEM characterization further revealed the sizes of these particles were around 18–39 nm in width (Fig. 1f).

Adjusting electronic structure of active site via electron transfer between interface of two phase on electrode was critical for activity, like built-in electric field [14] and strong metal support interaction [19–21]. To confirm if CoO and Cu foam could build interfacial electric filed for electron transfer, DFT calculation and XPS analysis were conducted. DFT calculation was used to investigate band structure of CoO and Cu, respectively. From Fig. 2a, S2 and S3, it was observed that the value band maximum (VBM) and conduction band minimum (CBM) of CoO were at 1.37 eV and − 0.23 eV (Criterion was fermi level (E_f) of CoO), respectively. E_f of Cu (1.09 eV) was between the VBM and CBM of CoO. The difference of energy band ($\triangle E = 1.32$ eV) between E_f of Cu and VBM of CoO generated interfacial electric field to transfer electron from Cu to CoO (Fig. 2a). The deference of energy band was crucial for producing interfacial electric field, and it has been reported that difference of energy band between tetrakis (4-carboxyphenyl) zinc porphyrin (ZnTCPP) and tetrakis (4-hydroxyphenyl) porphyrin (THPP) to form interfacial electric field to boost electron transfer from CBM of THPP to VBM of ZnTCPP for enhancement of hydrogen evolution [18].

XPS analysis was performed to further identify this electron transfer via position of binding energy [10]. Fig. 2b showed the Cu 2p orbital of CoO/Cu foam electrode, and found that two fitted peaks where 932.87 eV was Cu^0 and 934.97 was Cu(II) [38]. Compared to Cu foam with binding energy of Cu^0 at 932.68 eV, binding energy of Cu^0 in CoO/Cu foam shifted to higher energy by 0.19 eV (Fig. 2b), indicating that Cu lost some electrons. Fig. 2c was the XPS image of the Co 2p orbital in the unused CoO/Cu foam electrode, observing that the peak at 780.59 eV was the Co(II) 2p3/2 orbital, and the peak at 796.33 eV was Co(II) 2p1/2 orbital [39]. The other peaks at 785.69 eV and 803.22 eV were satellite peaks of Co(II) [39]. In contrast, binding energy of Co(II) in CoO/Cu foam moved to lower energy by 0.17 eV in comparison with binding energy of the Co(II) 2p1/2 orbital in the standard data database (National institute of standards and technology (NIST), 796.50 eV) [40], implying that CoO obtained electron from Cu. Thereby, it was concluded that CoO/Cu electrode constructed interfacial electric field to deliver electron from Cu foam to CoO. In addition, the responding O 1 s orbital of XPS picture in CoO/Cu electrode was shown in Fig. S4, and found that the peak at 529.97 eV was the Co-O bond and the peak at 531.53 eV belonged to -OH, respectively [39]. Moreover, according to the content analysis results of XPS, it can be known that Cu and Co occupied 6.36 % and 19.46 % on the surface of the CoO/Cu foam electrode, respectively,

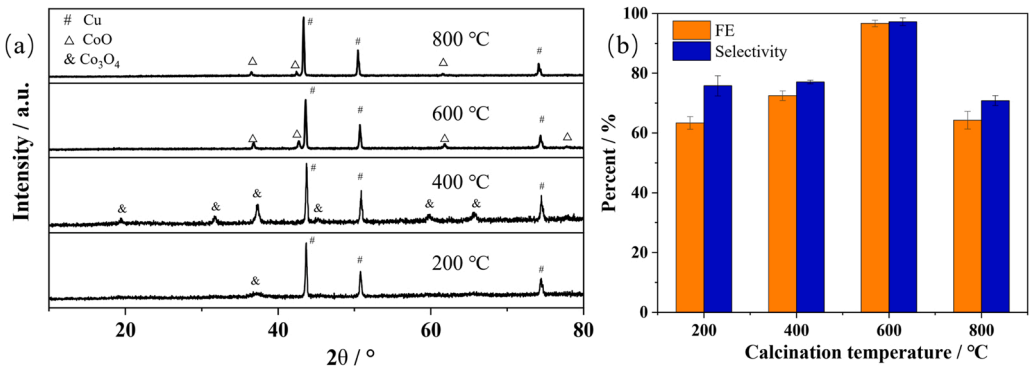

Fig. 3. (a) XRD spectra of electrodes under different calcination temperature; (b) FE (faraday efficiency) and NH_3 selectivity of electrodes synthesized via different calcination temperature. (Reaction conditions: 0.4 mol L^{-1} Na_2SO_4, 0.04 mol L^{-1} NO_3^-, potential of −1.2 V vs. Ag/AgCl).

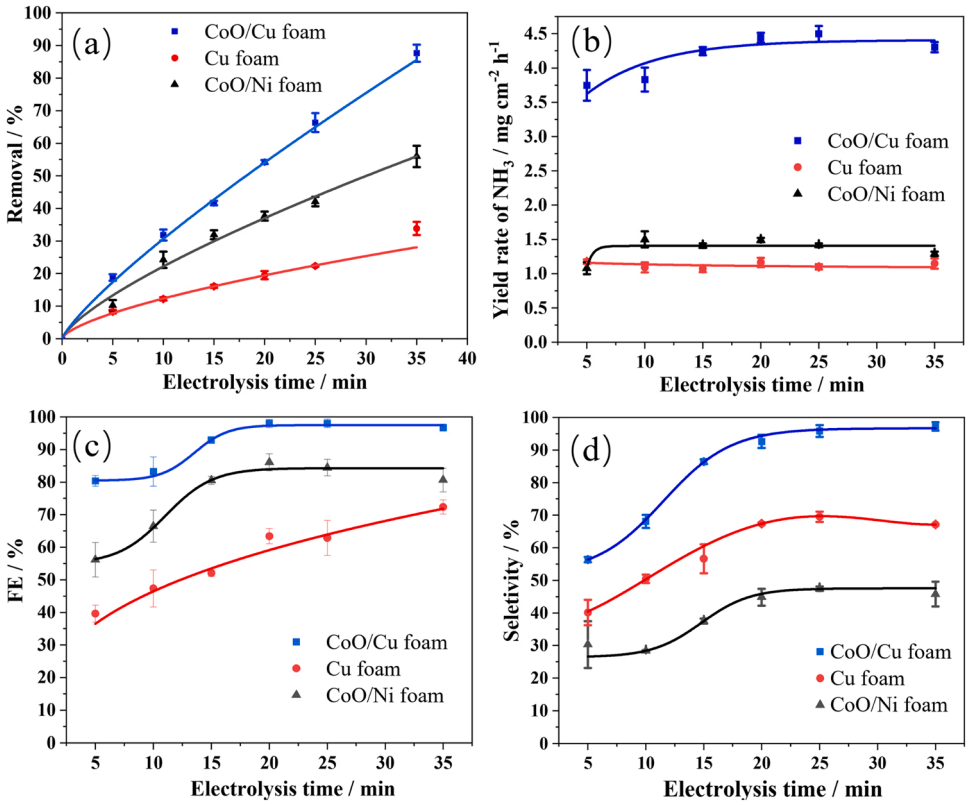

Fig. 4. (a–d) The change of nitrate removal, ammonia yield rate, FE and NH_3 selectivity along with electrolysis time in ERNA on CoO/Cu foam, Cu foam electrodes and CoO/Ni foam electrodes, respectively. (Reaction conditions: 0.4 mol L^{-1} Na_2SO_4, 0.04 mol L^{-1} NO_3^-, potential of −1.2 V vs. Ag/AgCl).

proving that CoO was successfully loaded on Cu foam and 6.36 % of Cu was exposed on the electrode surface, forming dual active sites. In addition, Cu LMM pictures uncovered that Cu^0 (568.5) and Cu(II) (568.9 eV) were in CoO/Cu foam electrode in Fig. S5 [41], and illustrated that Cu^0 was active sites in ERNA [10].

3.2. ERNA Performance of CoO/Cu foam

To ensure the excellent ERNA performance of the CoO/Cu foam electrode, the calcination temperature for electrode preparation was optimized at first. Fig. 3a showed the XRD patterns of the electrodes obtained at different calcination temperatures. There was a peak at 31.27° belonging to (220) crystal plane of Co_3O_4 (PDF#42-1467) except for three peaks of Cu foam (43.30, 50.43 and 74.13°) at the calcination temperature of 200 °C. As the calcination temperature increased to 400 °C, new peaks appeared at 19, 36.85, 38.54, 44.8, 59.35 and 65.23°, which belonged to (111), (311), (222), (400), (511) and (440) of Co_3O_4, respectively (Fig. 3a). Then, after the calcination temperature was further increased to 600 and 800 °C, only peaks of CoO appeared (Fig. 3a) except of peaks of Cu, indicating that Co_3O_4 was gradually converted into CoO with the increase of calcination temperature. Moreover, the corresponding nitrate removal increased from 73.3 % to 87.6 % when the calcination temperature increased from 200 °C to 600 °C, and then decreased to 80.1 % when it further increased to 800 °C (Fig. S6). The corresponding selectivity, faradic efficiency (FE) and ammonia yield rate also have similar trends in Fig. 3b and S7. Thus, the calcination temperature of 600 °C was the best for ERNA performance with the ammonia yield rate of 4.3 mg cm^{-2} h^{-1} and FE of 96.7 %, respectively.

In addition, the reaction conditions for ERNA were also optimized. For potential of − 1.0 V vs. Ag/AgCl, the nitrate removal, selectivity and FE were only 60.4 %, 70.5 % and 65.5 % (Fig. S8). And then, ERNA activity of CoO/Cu electrode increased until the potential augmented to − 1.2 V vs. Ag/AgCl (Fig. S8 and S9). However, the nitrate removal, selectivity and FE of the CoO/Cu foam electrode were only 74.3 %, 61.5 % and 54.9 % (Fig. S8) when the potential further increased to − 1.4 V vs. Ag/AgCl due to the enhancement of hydrogen evolution reaction (lots of gas bubbles appeared on the surface of electrode). Thus, − 1.2 V vs. Ag/AgCl was proper for ERNA on the CoO/Cu foam electrode.

For different initial concentration of nitrate, the CoO/Cu foam electrode could achieve a high nitrate removal in a low concentration of nitrate. For 0.005 mol L^{-1} NO_3^-, the removal of 96.4 % could be achieved with a low selectivity of 12.7 %, FE of 6.1 % and ammonia yield rate of 0.08 mg cm^{-2} h^{-1} (Fig. S10 and S11), because − 1.2 V vs. Ag/AgCl was too negative for low concentrations of nitrate and side reaction of hydrogen evolution reaction (HER) was serious. On the contrary, when the concentration of nitrate was too high (0.06 mol L^{-1}), the CoO/Cu foam electrode could maintain high selectivity and FE (98.0 % and 97.1 %), but the removal was relatively low (54.7 %) with an ammonia yield rate of 4.1 mg cm^{-2} h^{-1} (Fig. S10 and S11). Thus, 0.04 mol L^{-1} NO_3^- was the most appropriate for CoO/Cu foam due to the best performance of ERNA.

To confirm the role of CoO and Cu in dual active sites on the CoO/Cu foam electrode in ERNA, it was significant to compare CoO/Cu foam, CoO/Ni foam (Ni foam wasn't active site in ERNA in Fig. S12 [42]) and Cu foam electrodes. Especially, comparing CoO/Cu foam with CoO/Ni foam electrode was used to confirm the role of Cu. XRD analysis identified that there were three peaks of CoO, Ni and NiO after loading CoO on Ni foam via the same method of synthesizing CoO/Cu foam (Fig. S13). From Fig. 4a, it was found that nitrate removal increased with the reaction time on all three electrodes. Compared to Cu foam and CoO/Ni foam, CoO/Cu eventually reached a maximum removal of 87.6 %, which was 53.7 % more than Cu foam and was 31.7 % more than CoO/Ni foam electrodes, respectively. The corresponding ammonia yield rate reached 4.3 mg cm^{-2} h^{-1} on CoO/Cu foam electrode at 35 min, which was 258 % and 231 % higher than that on Cu foam and

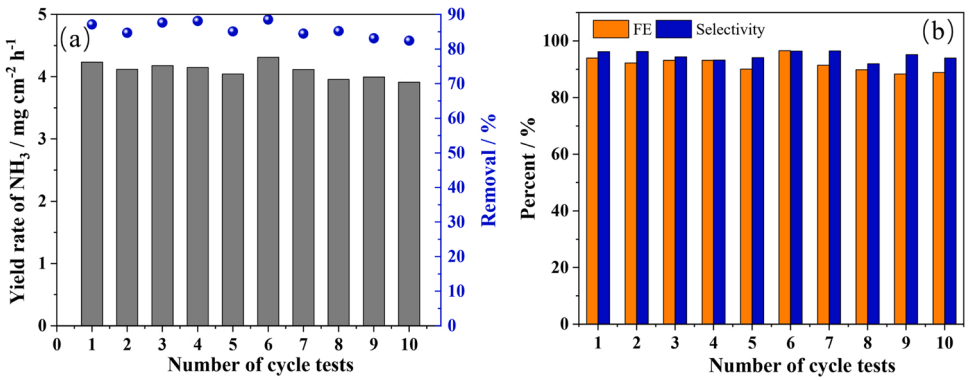

Fig. 5. (a, b) the variety of ammonia yield rate, nitrate removal, FE and selectivity of ammonia in 10 times cycle tests on CoO/Cu foam electrode. (Reaction conditions: 0.4 mol L^{-1} Na_2SO_4, 0.04 mol L^{-1} NO_3^-, potential of −1.2 V vs. Ag/AgCl).

CoO/Ni foam, respectively (Fig. 4b). Moreover, FE of CoO/Cu foam electrode finally reached 96.7 %, which was 24.3 % and 16.1 % higher than Cu foam and CoO/Ni foam, respectively (Fig. 4c).

Beside high removal, the excellent activity of CoO/Cu foam was attributed to high selectivity. As shown in Fig. 4d, CoO/Cu foam electrode obtained selectivity of 97.3 % at 35 min, whereas Cu foam only had 67.1 % and CoO/Ni foam was 45.7 %. And the amounts of total nitrogen (TN) barely changed along with electrolysis time on CoO/Cu foam electrode, indicating CoO/Cu foam electrode rarely produced nitrogenous gas in ERNA and ammonia in solution barely volatilized in ERNA (Fig. S14). In addition, ICP-MS detected that CoO/Cu foam and CoO/Ni foam electrodes had loaded 110 and 118 mg cm^{-2} Co, respectively. Thus, CoO and Cu foam were active sites of CoO/Cu foam electrode. Because CoO/Cu foam electrode belonged to CoO or Cu based electrodes, so it was significant to compare with other CoO or Cu based electrodes in previously reported paper. Notably, the selectivity of the CoO/Cu foam electrode exceed most of reported CoO and Cu based electrodes, and FE approached or surpassed many CoO and Cu based electrodes in high pH solution as well (Table S1, e. g. Cu/Cu_2O nanowire arrays electrode achieved FE of 95.8 % and selectivity of 81.2 % [10]; Cu/CuO_X/CF obtained FE of 93.58 % and selectivity of 95 % [26]; Pd octahedron electrode got FE of 35 % [43]), indicating that CoO/Cu foam electrode exhibited very high performance in ERNA.

In addition, the stability of the CoO/Cu foam electrode was also tested. From Fig. 5a, it was found that the nitrate removal maintained 88.5–82.4 % in the 10 cycle tests. Correspondingly, the highest ammonia yield was among 4.2–3.9 mg cm^{-2} h^{-1} (Fig. 5a). These suggested that CoO/Cu foam electrode kept stable removal and ammonia yield in 10 cycle tests. From Fig. 5b, it was showed that the change of the selectivity and FE of the CoO/Cu foam electrode in 10 cycle tests, and found that selectivity basically fluctuated among 96.5–92.0 % and FE changed between 94.1 % and 88.3 %. In addition, XRD analysis confirmed CoO/Cu foam only contained phase of CoO and Cu without other impurities after cycle tests (Fig. S15), and ICP-MS test confirmed that CoO/Cu foam electrode released little Co and Cu in solution (maximum amounts of Cu and Co were 3.4 and 5.3 μg L^{-1}, respectively, Fig. S16). In addition, XPS analysis was used to investigate interfacial electric field in CoO/Cu foam after cycle tests, and found that Cu positively moved and found that Cu positively increased 0.25 eV to attain 932.93 eV and CoO negatively shifted 0.12 eV to reach 796.38 eV (Fig. S17), indicating CoO/Cu electrode maintained interfacial electric field for electron transfer after cycle tests. Therefore, it was proved that the CoO/Cu foam electrode has a good stability and can be used for a long time in the ERNA.

3.3. *Effect of interfacial electric field on ERNA*

To reveal the effect of the interfacial electric field on the ERNA reactivity of CoO/Cu foam electrode, DFT calculations were carried on. In particular, previous literatures have reported that Cu and Cu_2O are the active species for ERNA reaction in Cu-based electrodes [10], so Cu (II) was not an active site, and thus Cu(II) was not considered in the model to save computing resource. Aforementioned energy band analysis and XPS measurements have been demonstrated the existence of interfacial electric field, and the bader charge analysis further uncovered the charge distribution of electrode. Fig. 6a showed that the average bader charge of Cu atoms in the interface of CoO/Cu foam was + 0.01 eV (Fig. 6a) and that of CoO in the interface of CoO/Cu foam was − 0.007 eV, indicating that the interfacial electric field had indeed transferred electrons from interfacial Cu to CoO, making Cu got positive charge and CoO took negative charge.

What's more, the adsorption of nitrate on electrode was further calculated. In the model of CoO/Cu foam electrode (Fig. 6a), one of the oxygen atoms in nitrate was adsorbed on the Cu atom of Cu foam, and

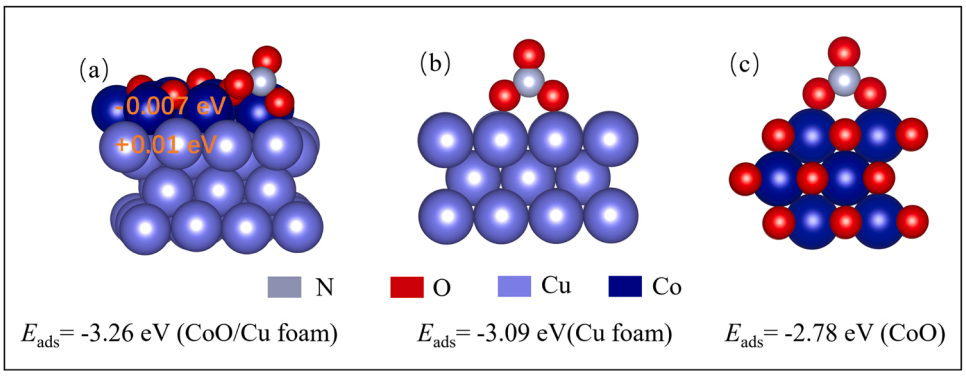

Fig. 6. (a–c) Structural diagrams of CoO/Cu foam, Cu foam and CoO for adsorption of nitrate.

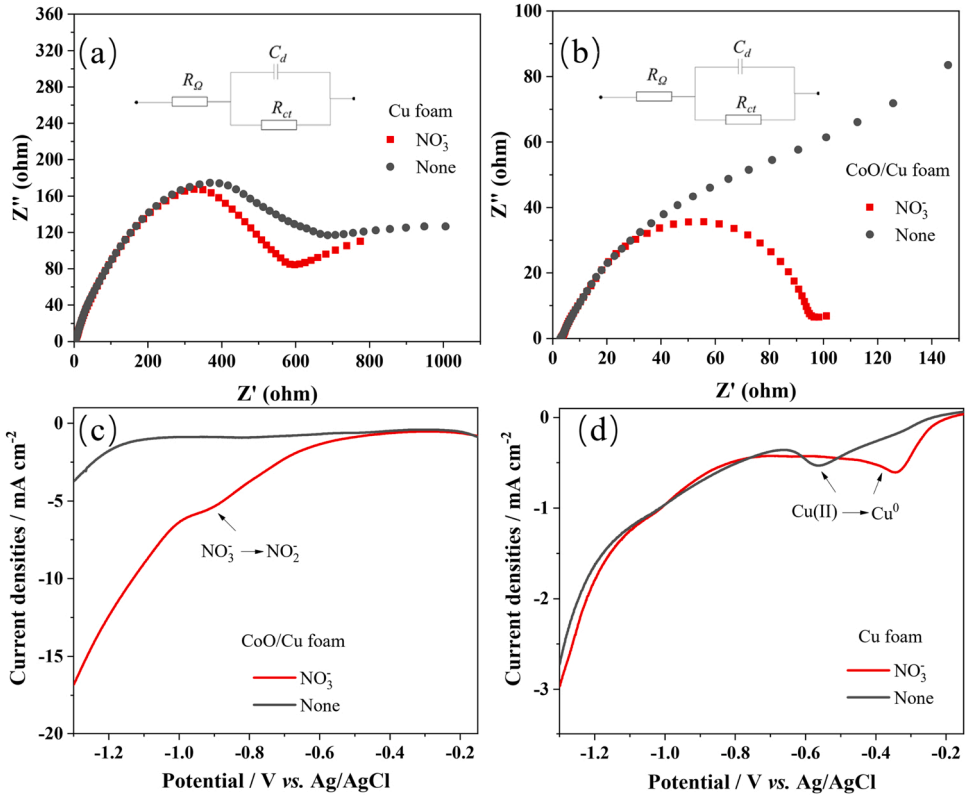

Fig. 7. (a, b) EIS pictures of Cu foam and CoO/Cu foam electrodes with NO_3^- or without (The inserted pictures of equivalent circuit diagram); (c, d) LSV pictures of CoO/Cu foam and Cu foam electrodes with NO_3^- or without.

another was adsorbed on the Co atom of CoO with the adsorption energy of − 3.26 eV. Moreover, Fig. 6b showed the structure of the Cu foam model for adsorbing nitrate, and it was observed that nitrate molecule was vertically adsorbed on the two Cu atoms of Cu foam through its two oxygen atoms, and the corresponding adsorption energy was − 3.09 eV. Fig. 6c exhibited the configuration of CoO adsorbing nitrate, and it was observed that CoO adsorbed nitrate by adsorption of two oxygen atoms of nitrates on two Co atom with adsorption energy of − 2.78 eV, which was weaker than Cu foam and CoO/Cu foam. Adsorption energy of nitrate on CoO/Cu foam was lower than Cu foam and CoO, indicating that CoO/Cu foam electrode realized strong adsorption of nitrate. On the one hand, strong adsorption could promote the adsorption and activation of nitrate. On the other hand, nitrate occupied the active sites, inhibiting the hydrogen evolution reaction to improve FE. Therefore, based on above results of XPS analysis and DFT calculation, it was proved that the interfacial electric field of CoO/Cu foam electrode let Cu atoms owned a small amount of positive charge, boosting the adsorption of nitrate.

Furthermore, since the improvement of adsorption of nitrate was beneficial for electron transfer, electrochemical impedance spectroscopy (EIS) tests were used to reveal the electron transfer during ERNA on the CoO/Cu foam and Cu foam electrodes. The EIS results of Cu foam showed that the charge transfer resistance (R_{ct}) obtained from equivalent circuit diagram decreased from 629.6 Ω to 525.8 Ω with a decrease of 16.5 % after adding nitrate (Fig. 7a). Moreover, R_{ct} of the CoO/Cu foam electrode was 158.3 Ω, and R_{ct} dropped to 86.3 Ω with a decline of 45.5 % after addition of nitrate (Fig. 7b). R_{ct} of the CoO/Cu foam was lower than Cu foam in ERNA (86.3 *vs.* 525.8 Ω), indicating CoO/Cu foam electrode increased electron transfer in ERNA.

In addition, LSV tests were conducted to study the kinetics of ERNA on CoO/Cu foam and Cu foam electrodes. For CoO/Cu foam electrode

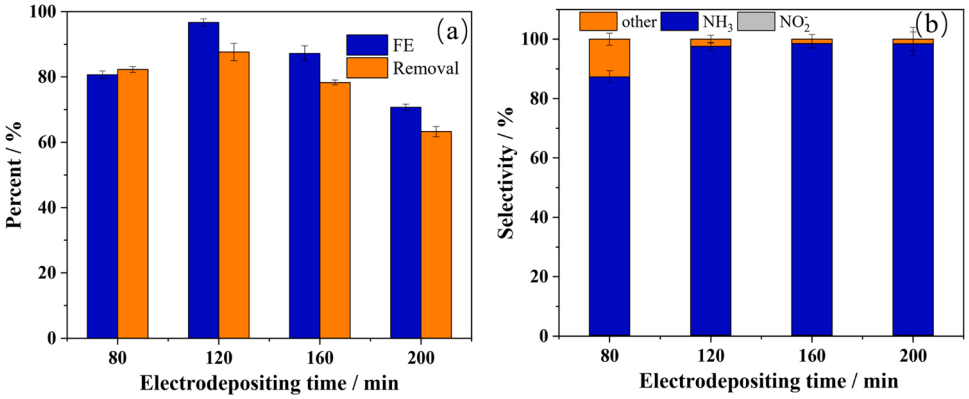

Fig. 8. (a, b) FE, nitrate removal and product selectivity (other, NH_3 and NO_2^-) of CoO/Cu foam electrodes obtained under different electrodepositing times, respectively. (Reaction conditions: 0.4 mol L^{-1} Na_2SO_4, 0.04 mol L^{-1} NO_3^-, potential of −1.2 V *vs.* Ag/AgCl).

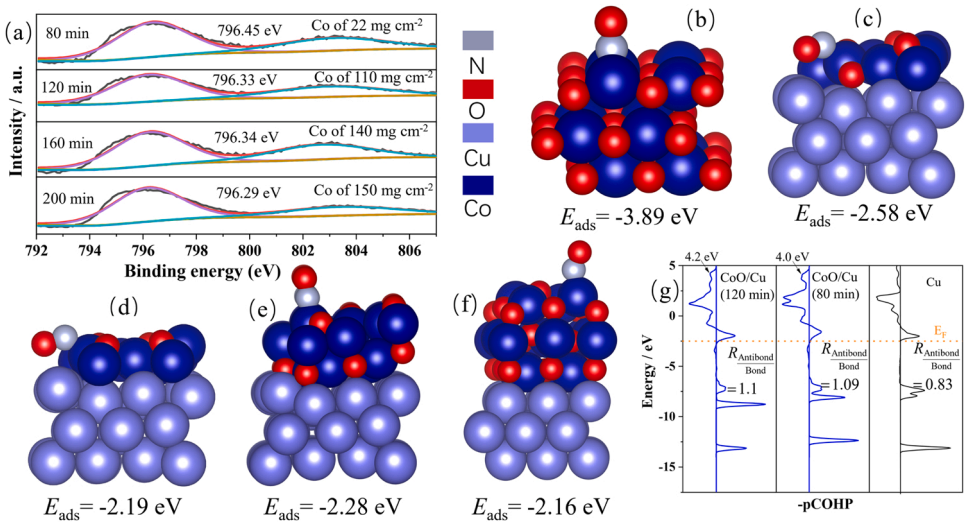

Fig. 9. (a) XPS images (Co 2p1/2 orbitals) of CoO/Cu foam electrodes obtained with different electrodeposition times; (b–f) Model structure diagrams of NO adsorption on CoO and CoO/Cu foam electrodes synthesized with electrodepositing time of 80, 120, 160 and 200 min, respectively. (g) Projected crystal orbital Hamilton population (pCOHP) of adsorbing NO on model of Cu foam, CoO/Cu foam with electrodepositing time of 80 and 120 min, respectively.

(Fig. 7c), the current density of LSV obviously increased than LSV without NO_3^- (−0.6 *vs.* −0.9 mA cm^{-2}) when potential was lower than − 0.48 V *vs.* Ag/AgCl, indicating that the ERNA began at − 0.48 V *vs.* Ag/AgCl. Next, the current density continually increased to 5.4 mA cm^{-2} to reach the peak of reducing NO_3^- to NO_2^- when potential reached − 0.89 V *vs.* Ag/AgCl (Fig. 7c). And then, the current density further increased for reducing NO_2^- when potential increased to lower potential (Fig. 7c). Similarly, ERNA started at − 1.1 V *vs.* Ag/AgCl Cu foam in Fig. 7d. However, the peak of reducing NO_3^- to NO_2^- disappeared since the current densities of hydrogen evolution reaction covered it, resulting in low ERNA activity and selectivity on Cu foam. In addition, the peaks at − 0.34 V *vs.* Ag/AgCl (with NO_3^-) and at − 0.56 V *vs.* Ag/AgCl (without NO_3^-) represented reduction of Cu(II) to Cu^0 on Cu foam in Fig. 7d. These results demonstrated that the interfacial electric field in CoO/Cu foam electrode promoted electron transfer via increasing adsorption of nitrate to enhance ERNA. In addition, cyclic voltammetry (CV) identified electrochemical surface area (ECSA) of CoO/Cu foam was 40.8 cm^2 cm^{-2} which was higher than Cu foam (3.1 cm^2 cm^{-2}) in Fig. S18, which was beneficial for reaction rate of ERNA.

Beside influence of the interfacial electric field on Cu in the CoO/Cu foam electrode, it also had an effect on CoO. The ratio of CoO and Cu foam on the surface of the CoO/Cu foam electrode can be controlled by the time of the electrodeposition precursor to investigate the effect of interfacial electric field on CoO. Firstly, the ICP-MS found the Co amounts of CoO/Cu foam with electrodepositing time of 80, 120, and 160 and 200 min were 22, 110, 140 and 150 mg cm^{-2}, respectively. The activity of the CoO/Cu foam electrodes obtained with different electrodeposition times was tested. As shown in Fig. 8a, the removal and FE separately increased from 82.3 % and 80.7 % to 87.6 % and 96.7 % when the electrodeposition time changed from 80 to 120 min, and then the removal and FE decreased to 63.3 % and 70.7 % of 200 min, respectively.

The ERNA performance of the CoO/Cu foam electrode prepared with electrodeposition time of 80 min was low due to its poor selectivity. There was still 12.6 % selectivity of other products on electrode with electrodeposition time of 80 min, while other electrodes obtained with electrode deposition time over 80 min had a selectivity of about 98 % (Fig. 8b). A good linear relationship between the amounts of Co and NH_3 selectivity (Fig. S19, $R^2 = 0.95$) indicated that ammonia selectivity was related to the amounts of Co in CoO/Cu foam electrode. Eventually, the highest ammonia yield was gained on the CoO/Cu foam with the electrodeposition time of 120 min, reaching 4.3 mg cm^{-2} h^{-1}, whereas the lowest ammonia yield of 3.08 mg cm^{-2} h^{-1} was obtained with electrodeposition time of 200 min (Fig. S20), suggesting that exceed CoO was bad for reaction rate due to the lack of enough exposure Cu foam. Thus, the loading amounts of 110 mg cm^{-2} Co on CoO/Cu foam with electrodepositing time of 120 min was beneficial for ERNA.

What's more, the electronic structure and ratios of Co and Cu on the CoO/Cu foam electrodes at different electrodeposition time were determined by XPS characterization. When the electrodeposition time increased from 80 to 200 min, Co/Cu ratio increased significantly from 2.55 to 29.89 when the amounts of Co raised from 22 to 150 mg cm^{-2} (Fig. 9a and Table S2). Notably, CoO basically covered the Cu foam when the electrodeposition time reached 200 min because of surface-exposed Cu atom content of only 0.83 %. However, the ERNA activity of the CoO/Cu foam electrode prepared by electrodeposition time of 200 min was not high and electrodeposition time of 120 min with Co/Cu ratio of 3.05 was proper for ERNA (Fig. 8a and b), indicating that single CoO didn't show good activity in ERNA, and both CoO and Cu foam worked on ERNA to achieve better activity. Moreover, XPS characterization also explored the effect of the interfacial electric field on the electronic structure of CoO in CoO/Cu foam electrode. When the electrodeposition time was longer, the fitting peak of Co(II) in CoO shifted to a low binding energy, and basically maintained around 796.32 eV after more than 120 min (Fig. 9a), which was lower than 796.45 eV of 80 min, indicating that the more CoO was deposited, the more electrons were obtained by Co(II). But, when the deposition time was too long, Co (II) didn't obtain more electron from Cu foam.

More important, DFT calculations revealed the effect of interfacial electric field on the adsorption of NO intermediates since adsorption strength of NO was critical for selectivity of NH_3 [30]. Models of CoO and CoO/Cu foam electrodes obtained with different electrodeposition time were simulated based on the results of XPS and XRD characterization. Fig. 9b showed the structure of adsorbing NO on CoO with adsorption energy of − 3.89 eV. Moreover, Fig. 9c exhibited the model of the CoO/Cu foam electrode prepared by electrodeposition time of 80 min, and found NO were adsorbed on CoO/Cu in structure of lying flat with the adsorption energy of − 2.58 eV. Similarly, flat NO was also adsorbed on the CoO/Cu model with electrodepositing time of 120 min, and the corresponding adsorption energy was − 2.19 eV (Fig. 9d). However, adsorption configurations of NO on CoO/Cu foam electrode models with electrodeposition time of 160 min and 200 min were different from 80 and 120 min, and NO molecules were adsorbed on model of electrode with upright structure, and the corresponding

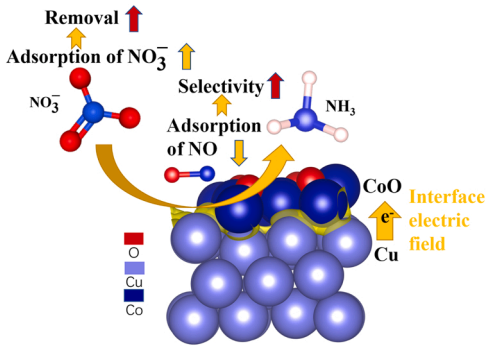

Fig. 10. Schematic diagram of the principle of regulating the interfacial electric field to enhance the ERNA activity on the dual active site CoO/Cu foam electrode.

adsorption energies were − 2.28 eV and − 2.16 eV (Fig. 9e and f). The adsorption energy of NO on all CoO/Cu electrodes were more positive than CoO, indicating that CoO decreased adsorption of NO after depositing itself on Cu foam due to the effect of the interfacial electric filed. What's more, the adsorption of NO on CoO/Cu foam with electrodepositing time of 120, 160 and 200 min were lower than that of 80 min, implying that the more electrons were CoO obtained, the more the adsorption strength of NO could be reduced. The adsorption strength was usually decided by electronic structure, and thus projected crystal orbital Hamilton population (pCOHP) analysis was carried on. From Fig. 9g, it was found that antibonding orbital in model of CoO/Cu adsorbing NO obtained more electrons over pure CoO because of higher ratio of antibonding electrons and bonding electrons ($R_{\frac{\text{Antibond}}{\text{Bond}}}$). What's more, CoO/Cu foam with electrodepositing time of 120 min has higher energy of anti-bonding orbital (4.2 vs. 4.0 eV, Fig. 9g) in model of adsorbing NO, indicating that more CoO depositing on Cu can provide more electron to fill more and higher antibonding orbital of adsorbing NO. More and Higher antibonding orbital in model of adsorbing NO on CoO/Cu foam electrodes could decrease adsorption of NO, and previous literatures reported that the weak adsorption of NO was favorable for producing ammonia to increase the selectivity of nitrate reduction [16]. Therefore, based on the above analysis, it was demonstrated that the interfacial electric filed in the CoO/Cu foam electrode with Co loading amounts of 110 mg cm^{-2} and Co/Cu ratio of 3.05 could decrease adsorption of NO to enhance selectivity of ammonia via providing electron to antibonding orbital of adsorbing NO, boosting ERNA (Fig. 10).

Besides, DEMS, in-situ FTIR and DFT calculations were used to elucidate the reaction pathway of ERNA on CoO/Cu foam electrode. The DEMS test also used a three-electrodes system at a potential of − 1.2 V vs. Ag/AgCl. As illustrated in Fig. 11a, the detected substances were NH, NH_2, NO and NH_3 with $m/z = 15$, 16, 30 and 17 without by-products H_2 ($m/z = 2$) and N_2 ($m/z = 28$) and other intermediates (HNO and NH_2OH), indicating that the ERNA on the CoO/Cu foam electrode was an indirect pathway (NO_3^-→*NO_3→*NO_2→NO→*N→*NH→*NH_2→*NH_3→NH_3). In addition, the amounts of N_2 or N_2O were measured via difference of initial total nitrogen (TN_0) and total nitrogen at reaction time t (TN_t) in solution due to the volatility of gas, and also demonstrated CoO/Cu foam barely generated nitrogenous gas (N_2 or N_2O) in Fig. S14. Moreover, in-situ FTIR found two peaks increased with reaction time in Fig. 11b, and 1638 cm^{-1} was O-H band of H_2O and 1098 cm^{-1} was N-H bond of NH_3 [44,45]. To further identify effect of active hydrogen (H*) in indirect reaction pathway on CoO/Cu foam electrode, H* scavenging experiment was conducted with scavenging agent of tertiary butyl alcohol (TBA). To avoid anodic oxidation of TBA, proton exchange membrane separated cathode and anode chamber. It was found that selectivity and FE decreased obviously from 95.8 % to 57.4% and 93.9% to 59.9%, respectively, when the concentration of TBA increased from 0 to 2 mM (Fig. 11c), suggesting that H* contributed much to selectivity of ammonia.

Furthermore, the variation of reaction energy along with the reaction pathway was studied by DFT calculation, and the corresponding adsorption structure of intermediates was shown in Fig. S21. It was

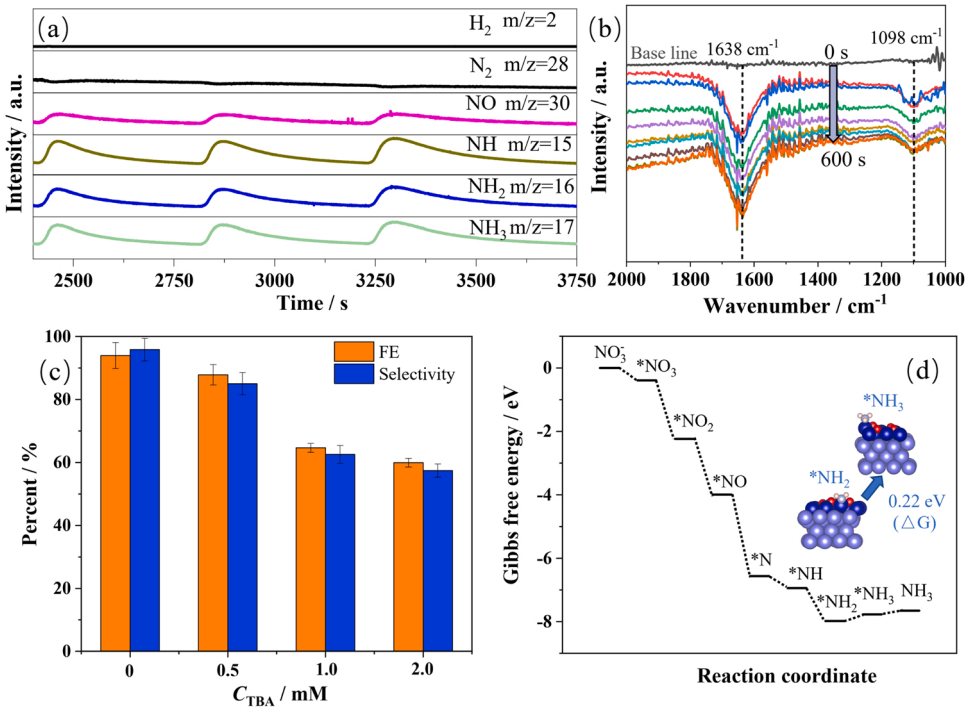

Fig. 11. (a, b) DEMS and in-situ FTIR results of ERNA on CoO/Cu foam electrode; (c) FE and selectivity of ammonia on CoO/Cu foam under different concentration of TBA (Tertiary butyl alcohol) (d) Variation of Gibbs free energy along with the reaction pathway during ERNA on CoO/Cu foam electrode. (Electrochemical reaction conditions: 0.4 mol L^{-1} Na_2SO_4, 0.04 mol L^{-1} NO_3^-, potential of −1.2 V vs. Ag/AgCl).

found the free Gibbs energy always deceased to − 7.98 eV on CoO/Cu foam electrode when reducing NO_3^- to $*NH_2$ (Fig. 11d), indicating that there was no energy barrier in the corresponding reaction step. However, the Gibbs free energy of $*NH_3$ rose to − 7.76 eV as $*NH_2$ was reduced to $*NH_3$ (Fig. 11d). Next, Gibbs free energy continued to lift to − 7.65 eV when $*NH_3$ was desorbed from the electrode surface to release NH_3 (Fig. 11d). The calculated energy barriers of the above two reaction steps were 0.22 and 0.11 eV, respectively, indicating that the potential rate-determining step (PRDS) of the ERNA on CoO/Cu foam electrode was $*NH_2 \rightarrow *NH_3$. Furthermore, the calculated energy of transition states (TS) in PRDS where reducing $*NH_2$ to $*NH_3$, unveiling that $*NH_2$ overcame energy barrier of TS of 0.46 eV to form $*NH_3$ in Fig. S22, and demonstrating $*NH_2 \rightarrow *NH_3$ was indeed PRDS in ERNA.

4. Conclusion

This study investigated the effect of the interfacial electric field on the ERNA for enhancing ERNA activity. The preparation method of CoO/Cu foam was electrodeposition with time of 120 min and calcination at 600 °C, and CoO/Cu foam electrode with loading Co of 110 mg cm^{-2} and Co/Cu ratio of 3.05 obtained the highest ammonia yield of 4.3 mg cm^{-2} h^{-1} with FE of 96.7 % and selectivity of 97.3 %. DFT calculation and XPS characterization demonstrated that the energy difference of E_f of Cu and VBM of CoO to form interfacial electric field to transfer electron from Cu foam to CoO, resulting in that Cu got positive charge of + 0.01 eV to increase adsorption of NO_3^- to promote nitrate removal while CoO got negative charge of − 0.007 eV to decrease adsorption of NO to improve selectivity for the enhancement of ERNA. In addition, DEMS, in-situ FTIR and DFT calculation proved that the pathway of ERNA on CoO/Cu foam electrode was an indirect reduction pathway, where the reduction of $*NH_2$ to $*NH_3$ was the potential rate-determining step. Thereby, it was believed that adjusting the interfacial electric field can optimize charge distribution of active site to increase ERNA activity, enabling efficient and sustainable nitrate removal and ammonia synthesis.

CRediT authorship contribution statement

Wenyang Fu: Conceptualization, Methodology, Formal analysis, Investigation, Data curation, Writing – original draft, Writing – review & editing. **Yingying Du:** Methodology, Formal analysis. **Jiana Jing:** Data curation. **Chunhong Fu:** Investigation. **Minghua Zhou:** Project administration, Funding acquisition, Resources, Conceptualization, Writing - review & editing.

Declaration of Competing Interest

The authors declare that they have no known competing financial interests or personal relationships that could have appeared to influence the work reported in this paper.

Data Availability

Data will be made available on request.

Acknowledgments

This work was financially supported by Tianjin Development Program for Innovation and Entrepreneurship, National Natural Science Foundation of China (21976096, 52170085 and 21773129), National High-level Foreign Experts Project (QN20200002003, G2021125001 and G2021125002), Tianjin Post-graduate Students Research and Innovation Project (2020YJSB048), and Fundamental Research Funds for the Central Universities, Nankai University. The authors also thanked Dr. Guangming Jiang for the assistance in DEMS analysis.

Appendix A. Supporting information

Supplementary data associated with this article can be found in the online version at doi:10.1016/j.apcatb.2022.122201.

References

[1] Y. Wang, C. Wang, M. Li, Y. Yu, B. Zhang, Nitrate electroreduction: mechanism insight, in situ characterization, performance evaluation, and challenges, Chem. Soc. Rev. 50 (2021) 6720–6733.
[2] X. Zhang, Y. Wang, C. Liu, Y. Yu, S. Lu, B. Zhang, Recent advances in non-noble metal electrocatalysts for nitrate reduction, Chem. Eng. J. 403 (2021), 126269.
[3] P.H. van Langevelde, I. Katsounaros, M.T. Koper, Electrocatalytic nitrate reduction for sustainable ammonia production, Joule 5 (2021) 290–294.
[4] X.T. Ju, C.L. Kou, F.S. Zhang, P. Christie, Nitrogen balance and groundwater nitrate contamination: comparison among three intensive cropping systems on the North China Plain, Environ. Pollut. 143 (2006) 117–125.
[5] W. Zheng, L. Zhu, Z. Yan, Z. Lin, Z. Lei, Y. Zhang, H. Xu, Z. Dang, C. Wei, C. Feng, Self-activated Ni cathode for electrocatalytic nitrate reduction to ammonia: from fundamentals to scale-up for treatment of industrial wastewater, Environ. Sci. Technol. 55 (2021) 13231–13243.
[6] R. Chauhan, V.C. Srivastava, Electrochemical denitrification of highly contaminated actual nitrate wastewater by Ti/RuO_2 anode and iron cathode, Chem. Eng. J. 386 (2020), 122065.
[7] G.-F. Chen, Y. Yuan, H. Jiang, S.-Y. Ren, L.-X. Ding, L. Ma, T. Wu, J. Lu, H. Wang, Electrochemical reduction of nitrate to ammonia via direct eight-electron transfer using a copper–molecular solid catalyst, Nat. Energy 5 (2020) 605–613.
[8] Q. Hu, Y. Qin, X. Wang, H. Zheng, K. Gao, H. Yang, P. Zhang, M. Shao, C. He, Grain boundaries engineering of hollow copper nanoparticles enables highly efficient ammonia electrosynthesis from nitrate, CCS Chem. 4 (2021) 2092–2103.
[9] T. Hu, C. Wang, M. Wang, C.M. Li, C. Guo, Theoretical insights into superior nitrate reduction to ammonia performance of copper catalysts, ACS Catal. 11 (2021) 14417–14427.
[10] Y. Wang, W. Zhou, R. Jia, Y. Yu, B. Zhang, Unveiling the activity origin of a copper-based electrocatalyst for selective nitrate reduction to ammonia, Angew. Chem. Int. Ed. Engl. 59 (2020) 5350–5354.
[11] G.A. Cerrón-Calle, A.S. Fajardo, C.M. Sánchez-Sánchez, S. Garcia-Segura, Highly reactive Cu-Pt bimetallic 3D-electrocatalyst for selective nitrate reduction to ammonia, Appl. Catal. B: Environ. 302 (2022), 120844.
[12] C. Chen, K. Li, C. Li, T. Sun, J. Jia, Combination of Pd–Cu catalysis and electrolytic H_2 evolution for selective nitrate reduction using protonated polypyrrole as a cathode, Environ. Sci. Technol. 53 (2019) 13868–13877.
[13] H. Wang, Q. Mao, T. Ren, T. Zhou, K. Deng, Z. Wang, X. Li, Y. Xu, L. Wang, Synergism of interfaces and defects: Cu/oxygen vacancy-rich Cu-Mn_3O_4 heterostructured ultrathin nanosheet arrays for selective nitrate electroreduction to ammonia, ACS Appl. Mater. Interfaces 13 (2021) 44733–44741.
[14] W.J. Sun, H.Q. Ji, L.X. Li, H.Y. Zhang, Z.K. Wang, J.H. He, J.M. Lu, Built-in electric field triggered interfacial accumulation effect for efficient nitrate removal at ultra-low concentration and electroreduction to ammonia, Angew. Chem. Int. Ed. Engl. 60 (2021) 22933–22939.
[15] R. Jia, Y. Wang, C. Wang, Y. Ling, Y. Yu, B. Zhang, Boosting selective nitrate electroreduction to ammonium by constructing oxygen vacancies in TiO_2, ACS Catal. 10 (2020) 3533–3540.
[16] T. Yoshioka, K. Iwase, S. Nakanishi, K. Hashimoto, K. Kamiya, Electrocatalytic reduction of nitrate to nitrous oxide by a copper-modified covalent triazine framework, J. Phys. Chem. C 120 (2016) 15729–15734.
[17] J.X. Feng, J.Q. Wu, Y.X. Tong, G.R. Li, Efficient hydrogen evolution on Cu nanodots-decorated Ni_3S_2 nanotubes by optimizing atomic hydrogen adsorption and desorption, J. Am. Chem. Soc. 140 (2018) 610–617.
[18] J. Jing, J. Yang, W. Li, Z. Wu, Y. Zhu, Construction of interfacial electric field via dual-porphyrin heterostructure boosting photocatalytic hydrogen evolution, Adv. Mater. 34 (2022), 2106807.
[19] W. Al Zoubi, N. Nashrah, R. Putri, A. Allaf, B. Assfour, Y. Ko, Strong dual-metal-support interactions induced by low-temperature plasma phenomenon, Mater. Today Nano 18 (2022), 100213.
[20] L. Zhai, X. She, L. Zhuang, Y. Li, R. Ding, X. Guo, Y. Zhang, Y. Zhu, K. Xu, H.J. Fan, Modulating built-in electric field via variable oxygen affinity for robust hydrogen evolution reaction in neutral media, Angew. Chem. Int. Ed. Engl. 61 (2022), e202116057.
[21] J. Zhang, D. Zhu, J. Yan, C.-A. Wang, Strong metal-support interactions induced by an ultrafast laser, Nat. Commun. 12 (2021) 1–10.
[22] D. Duffy, J. Harding, A. Stoneham, A simulation of the NiO/Ag interface with point defects, Acta Metall. Et. Mater. 43 (1995) 1559–1568.
[23] J. Wang, C. Cai, Y. Wang, X. Yang, D. Wu, Y. Zhu, M. Li, M. Gu, M. Shao, Electrocatalytic reduction of nitrate to ammonia on low-cost ultrathin CoO_x nanosheets, ACS Catal. 11 (2021) 15135–15140.
[24] Q. Chen, J. Liang, L. Yue, Y. Luo, Q. Liu, N. Li, A.A. Alshehri, T. Li, H. Guo, X. Sun, CoO nanoparticle decorated N-doped carbon nanotubes: a high-efficiency catalyst for nitrate reduction to ammonia, Chem. Commun. 58 (2022) 5901–5904.
[25] W. He, J. Zhang, S. Dieckhöfer, S. Varhade, A.C. Brix, A. Lielpetere, S. Seisel, J. R. Junqueira, W. Schuhmann, Splicing the active phases of copper/cobalt-based catalysts achieves high-rate tandem electroreduction of nitrate to ammonia, Nat. Commun. 13 (2022) 1–13.

[26] H. Wang, Y. Guo, C. Li, H. Yu, K. Deng, Z. Wang, X. Li, Y. Xu, L. Wang, Cu/CuO_x in-plane heterostructured nanosheet arrays with rich oxygen vacancies enhance nitrate electroreduction to ammonia, ACS Appl. Mater. Interfaces 14 (2022) 34761–34769.
[27] S.Z. Andersen, V. Čolić, S. Yang, J.A. Schwalbe, A.C. Nielander, J.M. McEnaney, K. Enemark-Rasmussen, J.G. Baker, A.R. Singh, B.A. Rohr, A rigorous electrochemical ammonia synthesis protocol with quantitative isotope measurements, Nature 570 (2019) 504–508.
[28] J. Gao, B. Jiang, C. Ni, Y. Qi, X. Bi, Enhanced reduction of nitrate by noble metal-free electrocatalysis on P doped three-dimensional Co_3O_4 cathode: mechanism exploration from both experimental and DFT studies, Chem. Eng. J. 382 (2020), 123034.
[29] W. Duan, G. Li, Z. Lei, T. Zhu, Y. Xue, C. Wei, C.J.Wr Feng, Highly active and durable carbon electrocatalyst for nitrate reduction reaction, Water Res. 161 (2019) 126–135.
[30] S. Garcia-Segura, M. Lanzarini-Lopes, K. Hristovski, P. Westerhoff, Electrocatalytic reduction of nitrate: fundamentals to full-scale water treatment applications, Appl. Catal. B: Environ. 236 (2018) 546–568.
[31] G. Kresse, J. Furthmüller, Efficient iterative schemes for ab initio total-energy calculations using a plane-wave basis set, Phys. Rev. B 54 (1996) 11169.
[32] B. Hammer, L.B. Hansen, J.K. Nørskov, Improved adsorption energetics within density-functional theory using revised Perdew-Burke-Ernzerhof functionals, Phys. Rev. B 59 (1999) 7413.
[33] K. Mathew, R. Sundararaman, K. Letchworth-Weaver, T. Arias, R.G. Hennig, Implicit solvation model for density-functional study of nanocrystal surfaces and reaction pathways, J. Chem. Phys. 140 (2014), 084106.
[34] M. Fishman, H.L. Zhuang, K. Mathew, W. Dirschka, R.G. Hennig, Accuracy of exchange-correlation functionals and effect of solvation on the surface energy of copper, Phys. Rev. B 87 (2013), 245402.
[35] W. Fu, Z. Hu, Y. Du, P. Su, Y. Su, Q. Zhang, M. Zhou, Building dual active sites Co_3O_4/Cu electrode to break scaling relations for enhancement of electrochemical reduction of nitrate to high-value ammonia, J. Hazard. Mater. 434 (2022), 128887.
[36] R. Nelson, C. Ertural, J. George, V.L. Deringer, G. Hautier, R. Dronskowski, LOBSTER: Local orbital projections, atomic charges, and chemical-bonding analysis from projector-augmented-wave-based density-functional theory, J. Comput. Chem. 41 (2020) 1931–1940.
[37] D. Sheppard, P. Xiao, W. Chemelewski, D.D. Johnson, G.J.T.J. o.c.p, Henkelman, A generalized solid-state nudged elastic band method, J. Chem. Phys. 136 (2012), 074103.
[38] T. Ghodselahi, M. Vesaghi, A. Shafiekhani, A. Baghizadeh, M. Lameii, XPS study of the Cu@ Cu_2O core-shell nanoparticles, Appl. Surf. Sci. 255 (2008) 2730–2734.
[39] K. Zhang, X. Xia, S. Deng, D. Xie, Y. Lu, Y. Wang, J. Wu, X. Wang, J. Tu, N-doped CoO nanowire arrays as efficient electrocatalysts for oxygen evolution reaction, J. Energy Chem. 37 (2019) 13–17.
[40] B.J. Tan, K.J. Klabunde, P.M. Sherwood, XPS studies of solvated metal atom dispersed (SMAD) catalysts. Evidence for layered cobalt-manganese particles on alumina and silica, J. Am. Chem. Soc. 113 (1991) 855–861.
[41] I. Platzman, R. Brener, H. Haick, R. Tannenbaum, Oxidation of polycrystalline copper thin films at ambient conditions, J. Phys. Chem. C 112 (2008) 1101–1108.
[42] Y. Wang, A. Xu, Z. Wang, L. Huang, J. Li, F. Li, J. Wicks, M. Luo, D.-H. Nam, C.-S. Tan, Enhanced nitrate-to-ammonia activity on copper–nickel alloys via tuning of intermediate adsorption, J. Am. Chem. Soc. 142 (2020) 5702–5708.
[43] J. Lim, C.Y. Liu, J. Park, Y.H. Liu, T.P. Senftle, S.W. Lee, M.C. Hatzell, Structure sensitivity of Pd facets for enhanced electrochemical nitrate reduction to ammonia, ACS Catal. 11 (2021) 7568–7577.
[44] Y. Yu, C. Wang, Y. Yu, Y. Wang, B. Zhang, Promoting selective electroreduction of nitrates to ammonia over electron-deficient Co modulated by rectifying Schottky contacts, Sci. China Chem. 63 (2020) 1469–1476.
[45] P. Su, W. Fu, Z. Hu, J. Jing, M. Zhou, Insights into transition metal encapsulated N-doped CNTs cathode for self-sufficient electrocatalytic degradation, Appl. Catal. B: Environ. 313 (2022), 121457.